J Neurooncol (2013) 111:153–161
DOI 10.1007/s11060-012-1008-z

LABORATORY INVESTIGATION

Real-time multi-modality imaging of glioblastoma tumor resection and recurrence

Shawn Hingtgen · Jose-Luiz Figueiredo · Christian Farrar · Matthias Duebgen · Jordi Martinez-Quintanilla · Deepak Bhere · Khalid Shah

Received: 5 June 2012 / Accepted: 21 November 2012 / Published online: 16 December 2012

Abstract The lack of relevant pre-clinical animal models incorporating the clinical scenario of Glioblastoma multiforme (GBM) resection and recurrence has contributed significantly to the inability to successfully treat GBM. A multi-modality imaging approach that allows real-time assessment of tumor resection during surgery and non-invasive detection of post-operative tumor volumes is urgently needed. In this study, we report the development and implementation of an optical imaging and magnetic resonance imaging (MRI) approach to guide GBM resection during surgery and track tumor recurrence at multiple resolutions in mice. Intra-operative fluorescence-guided surgery allowed real-time monitoring of intracranial tumor removal and led to greater than 90 % removal of established intracranial human GBM. The fluorescent signal clearly delineated tumor margins, residual tumor, and correlated closely with the clinically utilized fluorescence surgical marker 5-aminolevulinic acid/porphyrin. Post-operative non-invasive optical imaging and MRI confirmed near-complete tumor removal, which was further validated by immunohistochemistry (IHC). Longitudinal non-invasive imaging and IHC showed rapid recurrence of multi-focal tumors that exhibited a faster growth rate and altered blood-vessel density compared to non-resected tumors. Surgical tumor resection significantly extended long-term survival, however mice ultimately succumbed to the recurrent GBM. This multi-modality imaging approach to GBM resection and recurrence in mice should provide an important platform for investigating multiple aspects of GBM and ultimately evaluating novel therapeutics.

Keywords Glioma · Image-Guided resection · *In vivo* imaging · Recurrence

Shawn Hingtgen and Jose-Luiz Figueiredo contributed equally to this work.

Electronic supplementary material The online version of this article (doi:10.1007/s11060-012-1008-z) contains supplementary material, which is available to authorized users.

S. Hingtgen · J.-L. Figueiredo · M. Duebgen · J. Martinez-Quintanilla · D. Bhere · K. Shah (✉)
Molecular Neurotherapy and Imaging Laboratory, Massachusetts General Hospital, Harvard Medical School, Boston, MA 02114, USA
e-mail: kshah@mgh.harvard.edu

C. Farrar
Department of Radiology, Massachusetts General Hospital, Athinoula A. Martinos Center for Biomedical Imaging, Harvard Medical School, Boston, MA 02114, USA

K. Shah
Department of Neurology, Massachusetts General Hospital, Harvard Medical School, Boston, MA 02114, USA

K. Shah
Harvard Stem Cell Institute, Harvard University, Cambridge, MA 02138, USA

Introduction

Glioblastoma multiforme (GBM) is the most common primary brain cancer in adults [1]. GBM is associated with extremely high morbidity and mortality due to the highly aggressive and invasive nature of the tumor. Current treatments for GBM are not curative, but consist of surgical tumor resection followed by radiation and/or chemotherapy [2]. The ultimate goal of the surgical intervention is the

complete removal of GBM tumor cells while preserving neurological function, and the benefit to patients is closely tied to the extent of surgical removal [3, 4]. However, despite the critical and central role surgical resection plays in clinical GBM treatment, most in vivo animal models of GBM fail to incorporate tumor resection [5, 6] and instead use only orthotopic human xenografts that develop into a single solid aggressive lesion [6, 7].

Due to the value of complete GBM resection on patient survival, tools that allow intra-operative image guided resection hold the potential to ensure the maximum achievable percentage of tumor is resected in each patient and are continuing to be integrated into clinical use [8, 9]. In a Phase III study, the use of the intra-operative 5-aminolevulinic acid (5-ALA), an imaging agent that is rapidly taken up by GBM cells where it is converted into highly fluorescent porphyrins increased the rate of complete GBM surgical resection by 50 % and doubled 6 month progression-free survival [9]. In addition to use as a surgical aid, imaging is extensively integrated into the clinical diagnosis and monitoring of patients suffering from GBM pre- and post-surgery [10, 11]. In experimental models, the real-time quantitative feedback on individual cells and tumor deposits afforded by molecular imaging is critical for ensuring that mouse models faithfully reproduce the key aspects of clinical GBM resection and recurrence. Therefore, both the extensive clinical incorporation of molecular imaging, and the high-resolution quantitative spatial/temporal feedback provided by molecular imaging demand the incorporation of imaging techniques to ensure development of the most accurate pre-clinical GBM models. Previously, we and others have reported the creation and utility of mouse models of GBM surgical resection [12–14], and showed post-surgical tumor volumes could be quantified using bioluminescence imaging (BLI). However, the use of molecular imaging techniques to guide GBM resection in mice and to serially track post-operative tumor re-growth post-resection has not been investigated.

In the current study, we sought to utilize intra-operative and non-invasive molecular imaging to develop and characterize a multi-modality imaging approach to GBM resection and re-growth in mice. Our results showed intra-operative fluorescence allowed guided intracranial GBM resection that could be validated by simultaneous 5-ALA imaging. The combination of post-operative magnetic resonance imaging (MRI), BLI, and histology to non-invasively assess tumor debulking and serially monitor re-growth at multiple resolutions revealed the dynamics of tumor re-growth and differences between pre- and post-operative GBMs.

Materials and methods

Cell lines and viral vectors

U87 human glioma cells (American Type Culture Collection, Manassas, VA) were cultured in DMEM (Invitrogen Carlsbad, CA) supplemented with 10 % heat-inactivated fetal bovine serum, 100 μg/mL penicillin, 100 μg/mL streptomycin. Lentiviral vector engineered to express GFP-Fluc fusion protein (LV-GFP-FLuc) [15], was packaged in 293T/17 cells using a helper virus-free packaging system as described previously [15]. GBM cells were transduced with LV-GFP-FLuc at varying multiplicity of infection (MOI) by incubating virions in a culture medium containing 4 μg/mL protamine sulfate (Sigma St. Louis, MO) and cells were visualized for GFP expression by fluorescence microscopy.

Fluorescence-guided tumor resection

Nude mice (6–8 weeks of age; Charles River Laboratories, Wilmington, MA) 25–30 g in weight were used for the intracranial xenograft GBM model. U87-GFP-FLuc were harvested at 80 % confluency and implanted stereotactically (5×10^5 cells) in the right frontal lobe 2 mM lateral to the bregma and 0.5 mM from the dura ($n = 48$). On the day of tumor resection, mice received intravenous injection of 5-ALA (6 mg/kg) to allow validation with 5-ALA imaging ($n = 5$). Following immobilization on a stereotactic frame mice were placed under an Olympus SZX10 microscope (Olympus, Center Valley, PA). Intraoperative microscopic white light, GFP, and 5-ALA images were captured throughout the procedure using with a DP-72 camera and CellSens software (Olympus). A midline incision was made in the skin above the skull exposing the cranium of the mouse. The intracranial xenograft was identified using GFP fluorescence. A small portion of the skull covering the tumor was surgically removed using a bone drill and forceps and the overlying dura was gently peeled back from the cortical surface to expose the tumor. The U87-GFP-FLuc tumor was surgically excised using a combination of surgical dissection and aspiration, and images of GFP were continuously captured to assess accuracy of GFP-guided surgical resection ($n = 26$). Pre- and post-operative images of 5-ALA accumulation were captured to assess accuracy of GFP imaging. The GFP and expression and 5-ALA derived porphyrin fluorescence were defined and quantified using Image J analysis software (NIH, Bethesda, MD). The RGB intraoperative images were loaded into the program and converted to 8-bit gray-scale before subtracting background fluorescence equivalently for all images (setting the threshold to 50 %

maximum intensity). The integrated density of the mean fluorescence was then quantified for both GFP and 5-ALA images. For comparison of image-guided and standard non-guided tumor volumes, a subset of mice ($n = 7$) underwent GBM resection without intra-operative GFP imaging and tumor resection was performed until the walls of the normal brain were visible in the resection cavity by white light illumination. Following tumor removal, the resulting resection cavity was copiously irrigated and the skin closed with 7–0 Vicryl suture (JAJ, New Brunswick, NJ). All experimental protocols were approved by the Animal Care and Use Committees at Massachusetts General Hospital.

In vitro bioluminescence and fluorescence

To determine the correlation between the number of the transduced cells and the bioluminescence signal, U87-GFP-FLuc were seeded in different concentrations and substrates for luciferase (1.5 μg/mL) were added to the medium. Luciferase activity was measured using a luminometer (Promega, Madison, WI). To visualize GFP fluorescence, U87-GFP-FLuc cells (1×10^5) were seeded in 12-well culture plates. GFP fluorescence was detected using an Olympus IX51 microscope (Olympus, Center Valley, PA). Images were captured using a DP-72 Olympus camera and CellSens software (Olympus).

In vivo multi-modality imaging

To determine the volumes of pre-resected, post-resected, and recurrent GBM, mice were imaged by FLuc bioluminescence imaging ($n = 48$, pre; $n = 38$ post, recurrent $n = 8$) and MRI ($n = 5$ pre, post, and recurrent). To image *Fluc*, mice were given an intraperitoneal injection of D-luciferin (1 mg/animal in 100 μL of saline), and photon counts were recorded 10 min after administration over 7 min of image acquisition using a cryogenically cooled high-efficiency CCD camera (Roper Scientific, Trenton, NJ). Mice were imaged on days 14, 11, and 2 day before resection, and days 2, 8, and 13 post-resection. Images were processed as previously described [15]. MRIs were acquired on days 10 and 1 before resection, and days 1, 8, and 15 post-resection. All experiments were performed on a 9.4 Tesla magnet (Magnex Scientific Ltd, Oxford, UK) equipped with a 60 mm inner diameter gradient coil (Resonance Research, Billerica, MA) and interfaced with a Bruker MRI console (Bruker Biospin, Billerica, MA). The gradient coil has a maximum strength of 1500 mT/m and a rise time of 100 μs. Images were acquired using a home built mouse head bird-cage coil. Mice were positioned on a custom made mouse cradle and anesthetized with 1.5 % isoflurane in 50/50 O_2/medical air mixture with total flow rate of 1200 mL/min. Contrast agent injections were performed using an intravenous tail vein catheter. The imaging protocol consisted of: localizer image, T2-weighted RARE (Rapid Acquisition with Refocused Echoes) image, multi-echo spin-echo image (T2 map), echo-planar imaging (EPI) diffusion weighted image (DWI), and T1-weighted RARE images acquired before and after injection of 50 μL of 100 mM Gd-DTPA ($\sim$0.2 mmol Gd/kg bodyweight). Tumor volumes were determined from the T2 hyperintense tumor region of the brain in T2-weighted RARE images. The RARE acquisition parameters were: TE = 10 ms, RARE factor = 8, TR = 2500 ms, NA = 4, FOV = 1.92 cm, matrix = 128 × 128 (in-plane resolution = 150 μm), 0.5 mm slice thickness, 11 image slices. The tumor apparent diffusion coefficient (ADC) was determined from diffusion-weighted echo-planar images (EPI). Spin-echo EPI images were acquired with seven different diffusion gradient b-values: 0, 100, 300, 600, 900, 1200, 1500 s/mM^2. EPI acquisition parameters were: TE = 24 ms, TR = 3000 ms, NA = 1, FOV = 1.92 cm, matrix = 128 × 128 (in-plane resolution = 150 μm), 0.5 mm slice thickness, 11 image slices. The apparent diffusion coefficient (ADC) maps were generated using an in-house written MATLAB program for fitting the natural log of the signal intensity as a function of gradient b-value. The vascular permeability to Gd-DTPA was qualitatively assessed using T1-weighted RARE images acquired after the injection of Gd-DTPA. The RARE acquisition parameters were: TE = 8.5 ms, RARE factor = 4, TR = 600 ms, NA = 4, FOV = 2.0 cm, matrix = 256 × 256 (in-plane resolution = 78 μm), 0.5 mm slice thickness, 11 image slices. *Ex vivo:* ex-vivo analysis on resected tumors was performed by (1) GFP-fluorescence imaging under the dissection scope, and (2) incubating tumors with 1.5 μg/mL D-luciferin in PBS and by bioluminescence imaging. Fluorescence tumor volumes were determined by Image J analysis software (National Institutes of Health, Bethesda, MD).

Tissue processing

Mice bearing tumors in the cranial window ($n = 5$), mice with resected tumors ($n = 5$), or mice with recurrent tumors ($n = 8$) were perfused with formalin and brains were removed and sectioned. The tissue sections were dehydrated in xylene and ethanol, immersed in PBS, and stained with hematoxylin and Eosin (H&E). Floating brain sections were immunostained with antibodies against human Ki67 (DAKO, Carpinteria, CA) or CD31 (AbCam, Cambridge, MA), followed by incubation with Alexa dye 555 nm secondary antibodies (Invitrogen). GFP-expressing tumor cells and Ki67 or CD31 immunostaining was visualized by confocal microscopy as described previously [15]. Photomicrographs of both fluorescence and H&E

slides were taken using the Olympus IX51 upright microscope attached to the DP-72 camera, and Ki67 and CD31 staining was quantified using Image J.

Statistical analysis

Data were analyzed by Student *t* test when comparing 2 groups and by ANOVA, followed by Dunnetts post-hoc test when comparing greater than 2 groups. Data were expressed as mean ± SEM and differences were considered significant at $P < 0.05$. Survival times of mice groups ($n = 5$/group) were compared using log-rank test.

Results

To allow simultaneous high-resolution fluorescence imaging for guided resection and non-invasive BLI to quantify the extent of resection, we first engineered human U87 GBM cells to express a GFP-FLuc fusion protein (U87-GFP-FLuc) and validated their GFP expression and light emission to cell number correlation in vitro (Supplementary Fig. 1). *In vivo* serial BLI confirmed efficient tumor engraftment and showed steady tumor growth of intracranial U87-GFP-FLuc GBMs through two weeks (Fig. 1a). Following surgical opening of the skin, the fluorescence through the intact cranium was sufficient to allow clear visualization of the tumor border and creation of a cranial window exposing the underlying U87-GFP-FLuc tumor (Fig. 1b). To validate the accuracy of the GFP positive tumor, we injected mice with 5-ALA, which has been previously shown to accurately define tumor margins and clinically guide surgery [8, 9]. 5-ALA-derived porphyrin fluorescence extensively co-localized with GFP and defined similar tumor borders in the pre-operative tumor deposit (Fig. 1c). A combination of epi-fluorescence microscopy, intra-operative GFP-excitation and surgical dissection allowed near total resection of the intracranial GBM (Supplementary Movie 1 and Movie 2) with only a small residual GFP-positive tumor deposits remaining at the border of the resection cavity (Fig. 1d). The co-localization of 5-ALA-derived porphyrin fluorescence and GFP signal confirmed the small GBM micro-deposits were malignant tissue (Fig. 1d). Quantitative analysis of pre- and post-operative GFP images revealed the GFP-guided surgical resection lead to greater than 95 % tumor removal (Fig. 1e), while ex vivo BL imaging of excised tumor tissue showed only small variations in the total quantity of tumor tissue removed between mice (Fig. 1f).

To quantitatively assess the extent of surgical tumor resection MR and BL imaging showed greater than 96 and 92 % resection respectively of the initial GBM mass with only multiple small remaining residual tumor deposits (Fig. 2a–d). Post-operative BLI further showed image-guided resection increased the extent of tumor resection (image-guided resection: 92 % of tumor removed; standard non-guided: 76 % of tumor removed) and decreased the variability compared to non-guided surgical debulking (Fig. 2e). Histology on brains of mice following resection confirmed near gross total resection, with few visible tumor cells remaining at the periphery of the resection cavity (Fig. 2f–g). These results demonstrate the intra-operative fluorescent imaging allows highly accurate surgical resection of intracranial GBM in mice, and post-operative non-invasive imaging can provide quantitative data on the extent of resection and location of residual tumor deposits.

Clinical evidence has shown GBM recurrence is typically rapid and occurs within 2 cm of the resection border [16, 17]. MR imaging 8 days post-surgery showed the small residual post-operative GBM deposits had grown markedly in size leading to multi-focal recurrence that developed into a large single tumor by day 15 post-resection (Fig. 3a). Quantitative serial BLI of mice post-resection showed similar results revealing a sevenfold increase in tumor volumes during the first 5 days post-resection, that increased to 26-fold by day 13 (Fig. 3b). Survival analysis revealed the surgical resection significantly extended animal survival, however the benefit was modest (32.5 days resected vs. 22.5 days no resection) before the animals succumbed to recurrent tumors (Fig. 3c). Both H&E staining and fluorescence microscopy performed on post-mortem cryo-sectioned tissue validated the imaging results showing the presence of a large recurrent tumor that was anatomically distinct from the pre-resection neoplasm (Fig. 3d–i; Supplementary Fig. 2). These results show residual post-resection GBM deposits lead to rapid multi-focal tumor recurrence that can be tracked in real-time using non-invasive imaging.

To assess the growth of resected and non-resected tumors, we followed tumor growth in mice that underwent surgical resection or were left untreated. Longitudinal BLI analysis showed tumor volumes were greater in recurrent tumors as compared to non-resected tumors (Fig. 4a), and regression analysis of growth curves revealed the slope of recurrent GBM was markedly greater than the slope of non-resected tumor growth (15.093-recurrent; 6.081-non-resected, Fig. 4a). IHC staining supported this finding, showing the levels of the proliferation marker Ki67 was twofold greater in recurrent tumors than non-resected tumor (Fig. 4b). Despite the increased proliferation rate detected in recurrent tumors, CD31 staining showed a 46 % reduction in blood vessel density in recurrent tumors

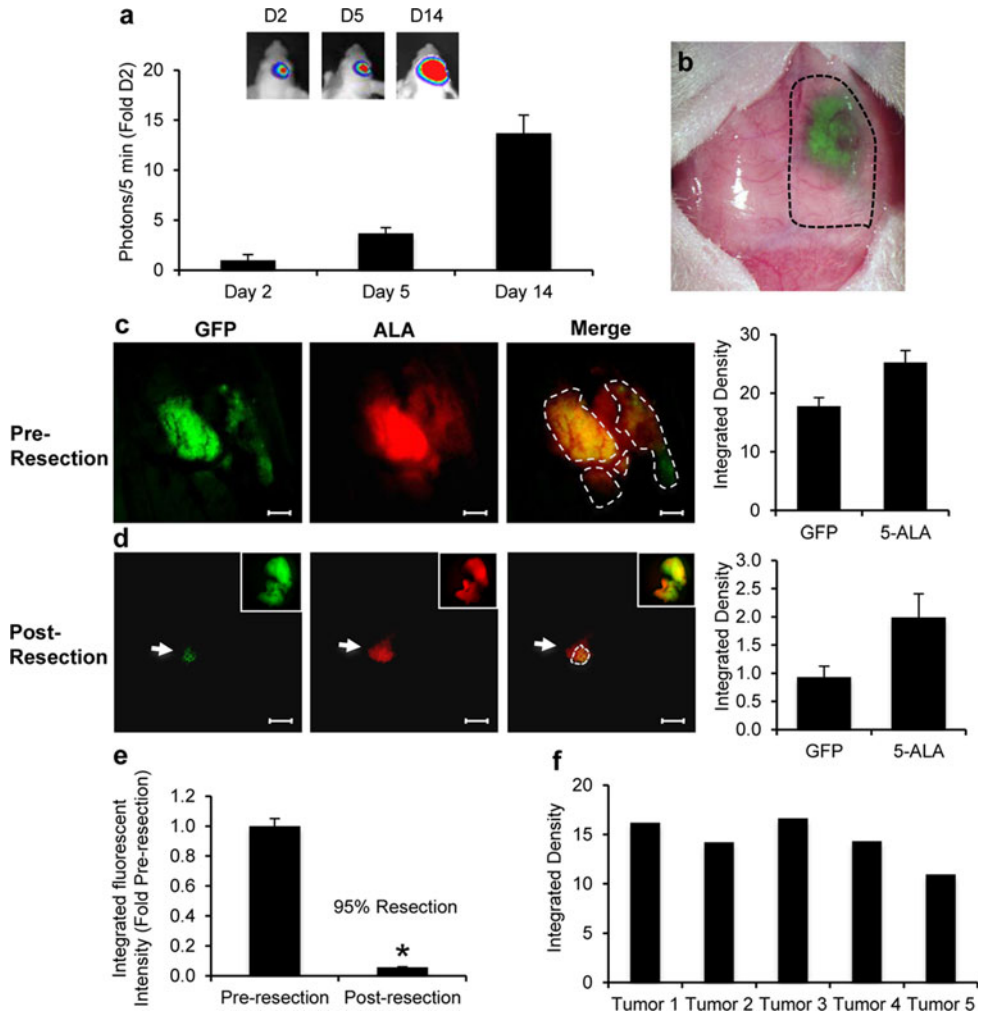

Fig. 1 Fluorescence-guided GBM resection and validation by 5-ALA. **a** Representative images and summary data showing the progression of orthotopic U87 human GBM in mice by BLI. **b** Representative image revealing the location of the U87-GFP-FLuc tumor visualized through the cranium. The borders of the cranial window were determined based on the fluorescent signature of the established tumor (depicted by *dashed line*). The craniotomy was then created to expose the underlying tumor. **c, d** Representative intra-operative fluorescent images of GFP-Fluc-expressing intracranial human GBM and validation by 5-ALA pre- **c** and post- **d** tumor resection. Insets depict GFP fluorescence, 5-ALA, or merged signal from excised tissue. Summary *graphs* demonstrating relative intra-cranial pre- and post- resection tumor volumes determined by GFP or 5-ALA imaging are shown. *Dashed line* shows area of co-localization between GFP and 5-ALA. **e** Summary *graph* demonstrating the extent of surgical resection determined by GFP fluorescence imaging. **f** Summary data showing the relative size of tumor tissue removed during surgical resection determined by GFP fluorescence imaging. Data are mean ± SD, $*P < 0.05$ determined by Students *t* test. *Scale bars* 200 μm

compared to non-resected tumors (Fig. 4c). Together, these results demonstrate tumor recurrence post-surgical resection occurs rapidly and tumors are distinct from the pre-resection tumor.

Discussion

In this study we present a molecular imaging approach to allow highly accurate surgical GBM resection and quantitative real-time tracking of multiple steps in GBM progression, resection, and recurrence. We show real-time intra-operative fluorescent imaging allows precise resection of GBM through cranial windows and quantification of tumor removal. Multi-modality non-invasive imaging and post-mortem IHC allowed tracking of tumor volumes post-resection and revealed differences in tumor growth of resected versus non-resected tumors.

The challenge of treating the aggressive and infiltrative GBM is highlighted by the fact that even surgical removal of a hemisphere is unable to extend patient survival beyond two years [18]. Although there is clear benefit from GBM surgery [4, 19], it remains unclear whether surgical debulking is able to extend long-term patient survival [20–23].

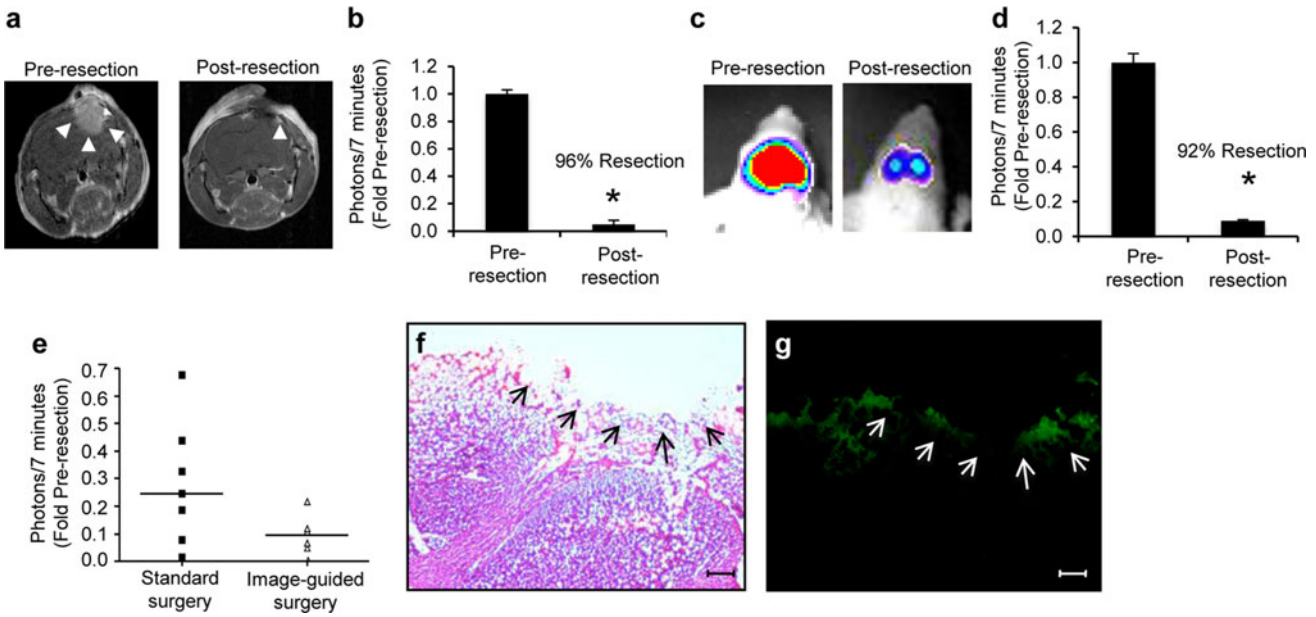

Fig. 2 Quantitative non-invasive imaging of GBM volumes pre- and post-resection. Representative images and summary data of quantitative imaging showing the extent of surgical resection by MRI (**a, b**) and BLI (**c, d**). MRI: one day before resection and one day post-resection, mice underwent MRI imaging following intravenous injection of Gd-DTPA. Tumor volumes were determined using Image J analysis software. *Arrows* indicate tumor deposits. BLI: one day before resection and one day post-resection, tumor volumes were assessed by injecting mice with D-luciferin and photon emission was determine over 7 min. **e** *Scatter plot* showing residual tumor volumes determined by BLI following image-guided resection or standard non-guided surgery. *Horizontal bar* shows mean of each surgery type. **f, g** Representative white light H&E images (**f**) and fluorescent photomicrographs (**g**) of corresponding brain sections post-resection (day 1). *Arrows* in **f** and **g** indicate extent of resection of the tumor. Data are mean ± SD, $*P < 0.05$ determined by Students *t* test. *Scale bars* 100 μm (**f**, **g**)

However, surgery remains a central component of the standard-of-care for GBM patients. Yet, most in vivo animal models of GBM fail to incorporate surgical resection, instead using only orthotopic human xenograft that develop into a solid aggressive lesion [6, 7]. Although limited, several previous studies have reported small animal models of GBM resection [12–14]. However, these models lacked tumor-specific removal by relying only on white light imaging. In the current study, we showed pre-operative fluorescent imaging was able to define the borders of the tumor through the intact cranium and allowed precise placement of cranial windows. During surgery, intra-operative GFP fluorescence imaging clearly identified tumor deposits and permitted highly accurate surgical removal of greater than 90 % of the GBM [13]. Further, we observed a close correlation between 5-ALA signal and GFP expression from engrafted U87-GFP-FLuc cells at all stages of surgery. Importantly, 5-ALA is one of the most common fluorescent labeling compounds used for GBM surgery in clinics as it leads to accumulation of fluorescing protoporphyrin IX in tumor tissue [24]. This suggests the incorporation of intra-operative fluorescence can increase the accuracy of surgical resection and that our model mimics the surgical resection in patients suggesting it can be used to further develop pre-clinical surgical resection models. Although intra-operative fluorescent imaging allows highly accurate definition of tumor location and subsequent resection, these parameters were challenging when performed using standard surgical methods. This underscores the benefit of intra-operative fluorescence during surgery in small animal models for improving accuracy and reproducibility.

The real-time quantitative feedback of individual cells and tumor deposits afforded by molecular imaging is an extremely powerful tool to faithfully reproduce many key aspects of GBM resection and recurrence in small animal models. This is vital for evaluating novel anti-GBM therapeutics, drug delivery modalities, and investigating aspects of GBM progression [15, 25–27]. In our study, post-operative MR and BL imaging revealed 96 and 92 % GBM removal respectively immediately following surgery. Serial MR imaging revealed multiple small tumor deposits post-surgery, and showed greater than a 50-fold increase in tumor volumes 8 days post-surgery and nearly 200-fold increase two weeks post-surgery. BLI confirmed the MR results, showing multiple tumors deposits following resection that lead to tenfold increases in tumor volumes by day 8 and 25-fold increase by day 25. In addition to the clinical relevance of MR, the increased resolution of MR can provide important structural information as well as

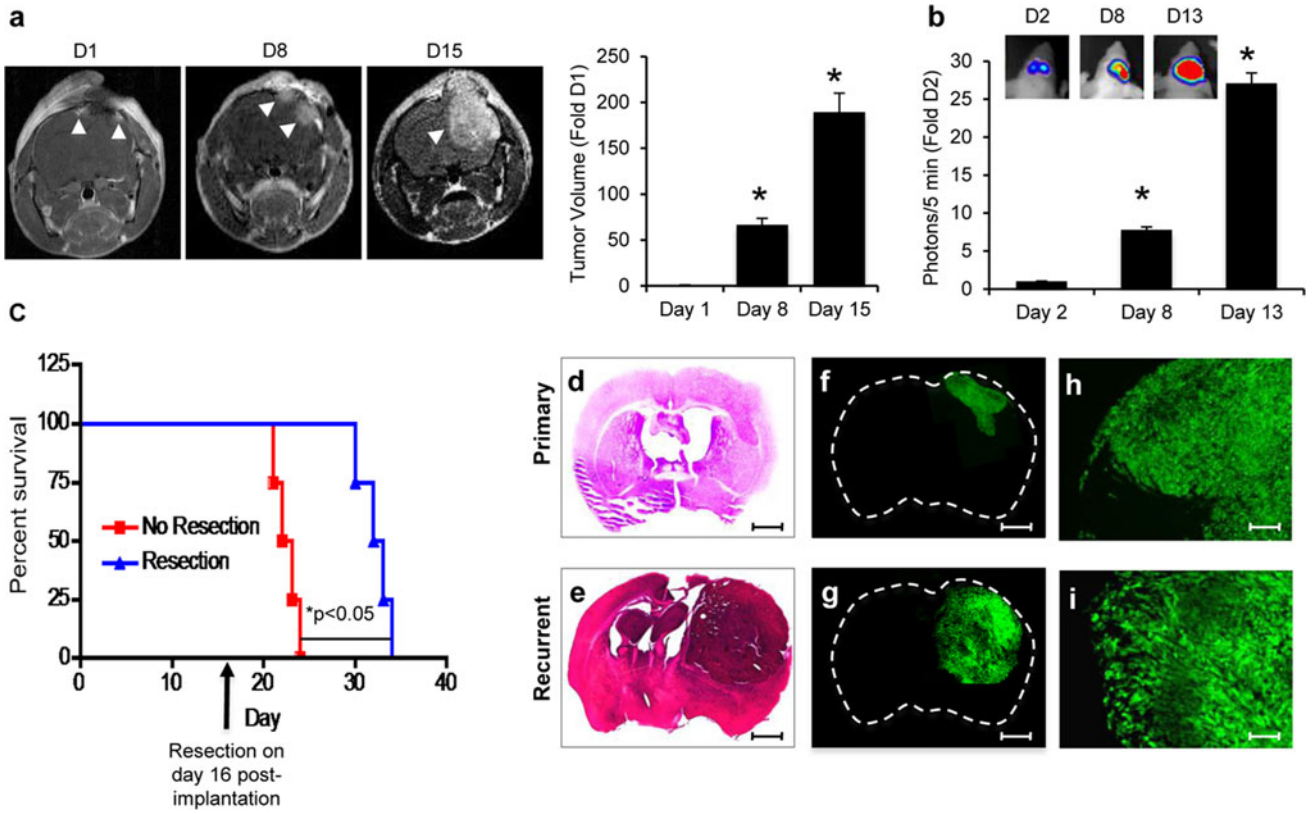

Fig. 3 Multi-modality tracking of post-operative GBM recurrence. **a,b** Representative images and summary graphs showing the recurrence of GBMs following surgical resection by non-invasive imaging. Following surgical debulking, mice were subjected to MRI on days 1, 8, and 15 post-resection (**a**) or BLI on day 2, 8, and 13 post-resection (**b**). *Arrows* indicate tumor deposits in panel (**a**). **c** Kaplan–meier curves depicting the survival of control without surgical resection or mice that underwent tumor debulking. **d–i** Representative white light H&E images (**d**, **e**) and fluorescent photomicrographs (**f–i**) of brain sections from primary tumor bearing mice (**d**, **f**, **h**) and from mice with recurrent tumors 2 weeks post-resection (**e**, **g**, **i**). Following intracranial xenograft, mice were sacrificed 2 weeks post-implantation, or underwent surgical debulking and sacrificed 2 week post-surgery to visualize tumor recurrence. ×2 magnification-**d**, **e**, **f**, **g**; ×10 magnification-**h**,**i**. Data are mean ± SD, $*P < 0.05$ determined by ANOVA (*panel a,b*), and log rank test (*panel c*). *Scale bars* 100 μm (**d**, **e**, **f**, **g**) and 400 μm (**h**, **i**)

quantitation of tumor volumes in three dimensions. Although not utilized clinically, serial BLI is ideal for pre-clinical studies allowing rapid serial imaging that is fully quantifiable and significantly cheaper. When combined with high-resolution fluorescence imaging, the results of these studies reveal a highly complimentary multi-modality imaging approach that could allow numerous questions to be answered simultaneously. Having validated the accuracy and efficiency of this approach in the current study, we aim at increasing the clinical relevance by addressing the challenges of using optical imaging to resect GBMs implanted deeper into the parenchyma in the region of the basal ganglia.

In this study, we utilized U87-GFP-FLuc human GBM that allowed the generation of a solid tumor that was necessary for efficient surgical resection, and lead to residual post-operative tumor deposits that were vital for studying GBM recurrence. Using this model, we observed recurrent U87-GFP-FLuc tumors showed a higher growth rate and Ki67 staining. Although the mechanism underlying the increased growth of recurrent GBM is unclear, the open cranium following resection that was absent in mice that did not undergo surgery may play a role. Therefore, growth rates of resected and non-resected GBM should be investigated in future studies where all animals receive craniotomies. In addition, inclusion of additional GBM cell lines and novel imaging modalities has the potential to increase the translatability of this model. Evidence has demonstrated that primary patient-derived GBM cell lines more faithfully recapitulate the clinical scenario of GBM [28, 29]. Furthermore, new MR and PET imaging techniques have the ability to improve accuracy of diagnosis and provide insights into the molecular signature of the GBM by allowing visualization of tumor metabolism, hypoxia, distribution of chemotherapies, and cerebral blood flow [30]. Studies such as these should ease the clinical translation of findings using small animal models of GBM resection.

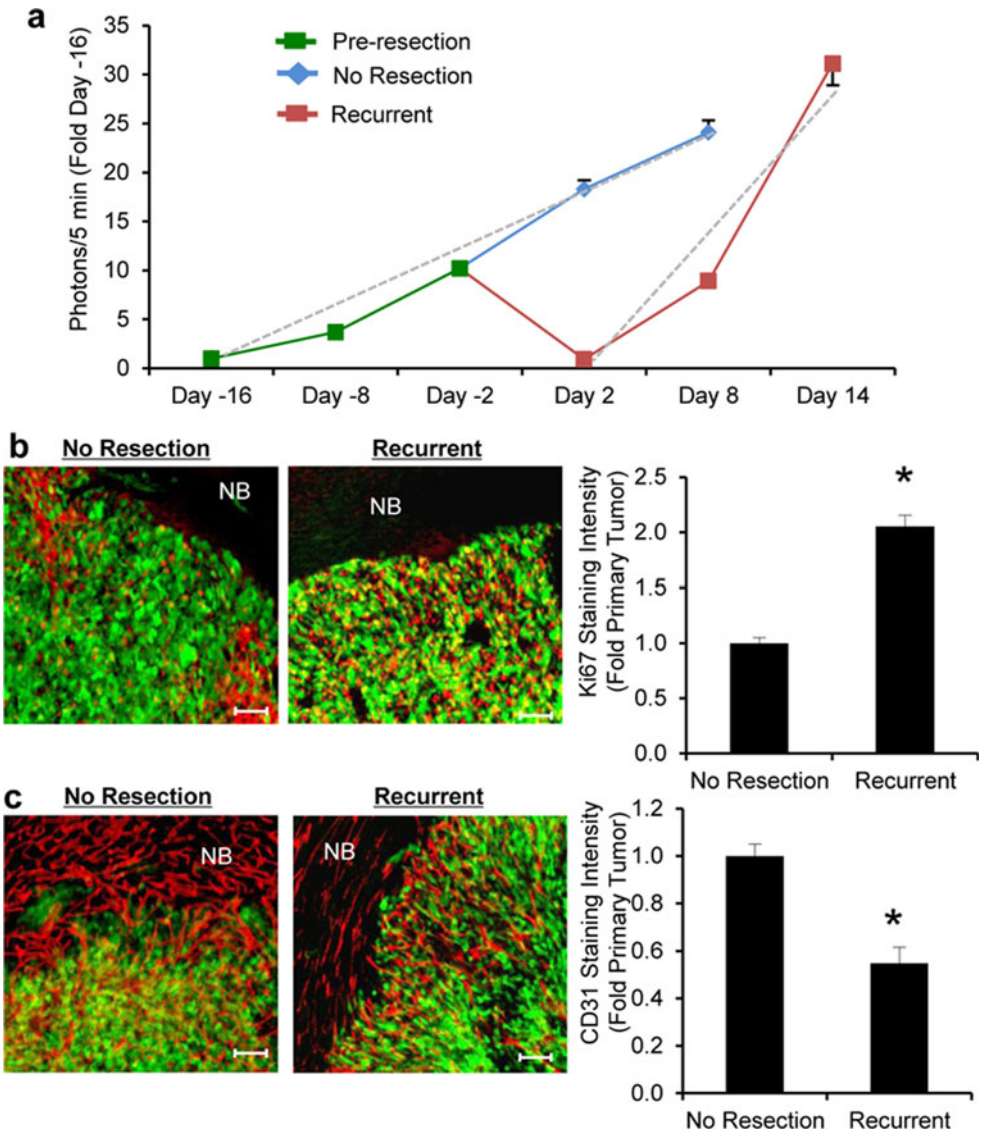

Fig. 4 Resected GBMs show higher growth rates than non-resected GBMs. **a** Summary graph showing the growth rates of primary or recurrent intracranial GBM determined by BLI. *Dotted line* shows the slope of the GBM growth curves for each group determined by regression analysis. **b, c** Representative images and summary data showing the relative expression levels of the proliferation marker Ki67 (**b**) and blood vessel marker CD-31 (**c**) in tissue sections from primary or recurrent GBM. Data are mean ± SD, $*P < 0.05$ determined by Students *t* test (panel b,c). *Scale bars* 100 μm

In conclusion, our studies demonstrate a new approach to developing pre-clinical mouse models of GBM surgical resection and recurrence that utilizes optical and MRI to assess multiple parameters before, during, and after surgery. Using this study as a template, we anticipate more accurate studies can be performed to evaluate potential new clinical therapeutics and drug delivery technologies that can be easily translated for treatment of patients following GBM resection.

Acknowledgments This work was supported by Alliance for Cancer Cell and Gene Therapy (KS), American Cancer Society (KS), James McDonald Foundation (KS) and National Institute of Health, R01-NSO71197 (KS).

Conflict of interest The authors have no conflicts to disclose.

References

1. Adamson C, Kanu OO, Mehta AI, Di C, Lin N, Mattox AK, Bigner DD (2009) Glioblastoma multiforme: a review of where we have been and where we are going. Expert Opin Investig Drugs 18: 1061–1083
2. Asthagiri AR, Pouratian N, Sherman J, Ahmed G, Shaffrey ME (2007) Advances in brain tumor surgery. Neurol Clin 25(4): 975–1003 Viii–ix
3. Lacroix M, Abi-Said D, Fourney DR, Gokaslan ZL, Shi W, DeMonte F, Lang FF, McCutcheon IE, Hassenbusch SJ, Holland E, Hess K, Michael C, Miller D, Sawaya R (2001) A multivariate analysis of 416 patients with glioblastoma multiforme: prognosis, extent of resection, and survival. J Neurosurg 95:190–198
4. Stark AM, Nabavi A, Mehdorn HM, Blomer U (2005) Glioblastoma multiforme-report of 267 cases treated at a single institution. Surg Neurol 63(2):162–169 discussion 169
5. Fomchenko EI, Holland EC (2006) Mouse models of brain tumors and their applications in preclinical trials. Clin Cancer Res 12:5288–5297

6. Jacobs VL, Valdes PA, Hickey WF, De Leo JA (2011) Current review of in vivo GBM rodent models: emphasis on the CNS-1 tumour model. ASN Neuro 3:e00063
7. Dai C, Holland EC (2001) Glioma models. Biochim Biophys Acta 1551:M19–M27
8. Krammer B, Plaetzer K (2008) ALA and its clinical impact, from bench to bedside. Photochem Photobiol Sci 7:283–289
9. Stummer W, Pichlmeier U, Meinel T, Wiestler OD, Zanella F, Reulen HJ (2006) Fluorescence-guided surgery with 5-aminolevulinic acid for resection of malignant glioma: a randomised controlled multicentre phase III trial. Lancet Oncol 7:392–401
10. Quant EC, Wen PY (2011) Response assessment in neuro-oncology. Curr Oncol Rep 13:50–56
11. Mehta AI, Kanaly CW, Friedman AH, Bigner DD, Sampson JH (2011) Monitoring radiographic brain tumor progression. Toxins (Basel) 3:191–200
12. Akbar U, Jones T, Winestone J, Michael M, Shukla A, Sun Y, Duntsch C (2009) Delivery of temozolomide to the tumor bed via biodegradable gel matrices in a novel model of intracranial glioma with resection. J Neurooncol 94:203–212
13. Kauer TM, Figueiredo JL, Hingtgen S, Shah K (2011) Encapsulated therapeutic stem cells implanted in the tumor resection cavity induce cell death in gliomas. Nat Neurosci 15(2):197–204
14. Bello L, Giussani C, Carrabba G, Pluderi M, Lucini V, Pannacci M, Caronzolo D, Tomei G, Villani R, Scaglione F, Carroll RS, Bikfalvi A (2002) Suppression of malignant glioma recurrence in a newly developed animal model by endogenous inhibitors. Clin Cancer Res 8:3539–3548
15. Shah K, Hingtgen S, Kasmieh R, Figueiredo JL, Garcia-Garcia E, Martinez-Serrano A, Breakefield X, Weissleder R (2008) Bimodal viral vectors and in vivo imaging reveal the fate of human neural stem cells in experimental glioma model. J Neurosci 28:4406–4413
16. Nieder C, Grosu AL, Molls M (2000) A comparison of treatment results for recurrent malignant gliomas. Cancer Treat Rev 26:397–409
17. Hou LC, Veeravagu A, Hsu AR, Tse VC (2006) Recurrent glioblastoma multiforme: a review of natural history and management options. Neurosurg Focus 20:E5
18. Hillier WF Jr (1954) Total left cerebral hemispherectomy for malignant glioma. Neurology 4:718–721
19. Kanaly CW, Ding D, Mehta AI, Waller AF, Crocker I, Desjardins A, Reardon DA, Friedman AH, Bigner DD, Sampson JH (2011) A novel method for volumetric MRI response assessment of enhancing brain tumors. PLoS One 6:e16031
20. Nazzaro JM, Neuwelt EA (1990) The role of surgery in the management of supratentorial intermediate and high-grade astrocytomas in adults. J Neurosurg 73:331–344
21. Quigley, Maroon JC (1991) The relationship between survival and the extent of the resection in patients with supratentorial malignant gliomas. Neurosurgery 29(3):385–388 discussion 388-389
22. Hess KR (1999) Extent of resection as a prognostic variable in the treatment of gliomas. J Neurooncol 42:227–231
23. Metcalfe SE, Grant R (2001) Biopsy versus resection for malignant glioma. Cochrane Database Syst Rev (3):CD002034
24. Stummer W, Stocker S, Novotny A, Heimann A, Sauer O, Kempski O, Plesnila N, Wietzorrek J, Reulen HJ (1998) In vitro and in vivo porphyrin accumulation by C6 glioma cells after exposure to 5-aminolevulinic acid. J Photochem Photobiol B 45:160–169
25. Hingtgen SD, Kasmieh R, van de Water J, Weissleder R, Shah K (2010) A novel molecule integrating therapeutic and diagnostic activities reveals multiple aspects of stem cell-based therapy. Stem Cells 28:832–841
26. Willmann JK, van Bruggen N, Dinkelborg LM, Gambhir SS (2008) Molecular imaging in drug development. Nat Rev Drug Discov 7:591–607
27. Heckl S, Pipkorn R, Nagele T, Vogel U, Kuker W, Voight K (2004) Molecular imaging: bridging the gap between neuroradiology and neurohistology. Histol Histopathol 19:651–668
28. Wakimoto H, Kesari S, Farrell CJ, Curry WT Jr, Zaupa C, Aghi M, Kuroda T, Stemmer-Rachamimov A, Shah K, Liu TC, Jeyaretna DS, Debasitis J, Pruszak J, Martuza RL, Rabkin SD (2009) Human glioblastoma-derived cancer stem cells: establishment of invasive glioma models and treatment with oncolytic herpes simplex virus vectors. Cancer Res 69(8):3472–3481
29. Giannini C, Sarkaria JN, Saito A, Uhm JH, Galanis E, Carlson BL, Schroeder MA, James CD (2005) Patient tumor EGFR and PDGFRA gene amplifications retained in an invasive intracranial xenograft model of glioblastoma multiforme. Neuro Oncol 7: 164–176
30. Taghva A, Khalessi AA, Kim PE, Liu CY, Apuzzo ML (2010) From atom to brain: applications of molecular imaging to neurosurgery. World Neurosurg 73:477–485